

# Development of multi-component diesel surrogate fuel models – Part II:Validation of the integrated mechanisms in 0-D kinetic and 2-D CFD spray combustion simulations

**Poon, Hiew Mun; Pang, Kar Mun; Ng, Hoon Kiat; Gan, Suyin; Schramm, Jesper**

*Published in:*
Fuel

*Link to article, DOI:*
10.1016/j.fuel.2016.04.114

*Publication date:*
2016

*Document Version*
Peer reviewed version

# Development of Multi-Component Diesel Surrogate Fuel Models - Part II: Validation of the Integrated Mechanisms in 0-D Kinetic and 2-D CFD Spray Combustion Simulations

Hiew Mun Poon[1], Kar Mun Pang[2], Hoon Kiat Ng[1*], Suyin Gan[3], Jesper Schramm[2]

[1] *Department of Mechanical, Materials and Manufacturing Engineering, The University of Nottingham Malaysia Campus, Jalan Broga, 43500 Semenyih, Selangor, Malaysia.*

[2] *Department of Mechanical Engineering, Danmarks Tekniske Universitet, Nils Koppels Allé, Bygning 403, 2800 Kgs. Lyngby.*

[3] *Department of Chemical and Environmental Engineering, The University of Nottingham Malaysia Campus, Jalan Broga, 43500 Semenyih, Selangor, Malaysia.*

* Corresponding author: Tel: +603 89248161; Fax: +603 89248017; Email-address: hoonkiat.ng@nottingham.edu.my (H.K. Ng)

## Abstract

The aim of this study is to develop compact yet comprehensive multi-component diesel surrogate fuel models for computational fluid dynamics (CFD) spray combustion modelling studies. The fuel constituent reduced mechanisms including n-hexadecane (HXN), 2,2,4,4,6,8,8-heptamethylnonane (HMN), cyclohexane (CHX) and toluene developed in Part I are applied in this work. They are combined to produce two different versions of multi-component diesel surrogate models in the form of MCDS1 (HXN + HMN) and MCDS2 (HXN + HMN + toluene + CHX). The integrated mechanisms are then comprehensively validated in zero-dimensional chemical kinetic simulations under a wide range of shock tube and jet stirred reactor conditions. Subsequently, the fidelity of the surrogate models is further evaluated in two-dimensional CFD spray combustion simulations. Simulation results show that ignition delay (ID) prediction corresponds well to the change of fuel constituent mass fraction which is calculated to match the cetane number (CN). In addition, comparisons of the simulation results to the experimental data of #2 diesel fuel (D2) in a constant volume

combustion chamber show that IDs and lift-off lengths are reasonably well replicated by the models. The MCDS2 model is also found to perform better in the soot formation prediction in D2 fuel combustion as the model contains aromatic and cyclo-alkane components which provide an additional pathway to the formation of rich species such as $C_2H_2$ and $C_6H_6$. Implementation of MCDS2 predicts an increase of maximum local soot volume fraction by a factor of 2.1 when the ambient temperature increases from 900K to 1000K, while the prediction by MCDS1 is lower at 1.6. This trend qualitatively agrees with the experimental observation. This work demonstrates that MCDS1 serves as a potential surrogate fuel model for diesel fuels with CN values ranging from 15 to 100. It also shows that MCDS2 is a more appropriate surrogate model for fuels with aromatics and cyclo-paraffinic contents, particularly when soot calculation is of main interest.

Keywords: multi-component diesel surrogate, CFD simulations, spray combustion, chemical kinetic mechanism, soot formation.

## 1. Introduction

In multi-dimensional computational fluid dynamics (CFD) modelling studies [1–6], n-heptane has been widely utilised as a single-component diesel surrogate fuel model owing to its cetane number (CN) of 55, which is comparable to those of the actual diesel fuels which range between 40 to 56 [7]. Nonetheless, actual diesel fuels generally consist of long carbon chain structure with 10 to 25 carbon atoms [7]. Fuels with long-chain n-alkanes exhibit higher reactivity at low temperatures as compared to those with short carbon chains. This is due to the higher ratio of secondary to primary hydrogen atoms which then increases the H-atom abstraction rate during the initiation phase of the oxidation of alkanes [8]. As a consequence, the combustion of long-chain hydrocarbons particularly n-hexadecane (HXN) [9] has become the centre of attention in many current research works [10–13]. HXN is the

primary reference fuel and it has a CN of 100. Surrogate fuel models with different CN values can hence be produced when HXN is blended with other fuels such as 1-methylnaphthalene with a CN of 0 and 2,2,4,4,6,8,8-heptamethylnonane (HMN) with a CN of 15. Therefore, HXN has been identified as a promising component for diesel fuel surrogate model in recent works [12–14]. Nonetheless, it is evident that the Hydrogen/Carbon Molar Ratio (H/C) of HXN is different from that of the actual diesel fuels, on top of the difference in CN. H/C ratio is a key property in simulation studies in order to replicate combustion properties such as heat of reaction, local air/fuel stoichiometric location, flame temperature and flame speed [15]. It is important to note that similar restriction is expected to hold for any other single-component diesel surrogate fuels [16,17].

Apart from that, the Polycyclic Aromatic Hydrocarbons (PAH) formation in diesel fuel combustion is not well described by a single-component diesel surrogate fuel model [7]. In the experiment carried out by Kook and Pickett [18], soot formation of a surrogate fuel comprising 23% m-xylene and 77% n-dodecane (by volume) was studied and the sooting tendency was subsequently compared to a conventional jet fuel under diesel-engine like conditions. Their planar laser induced incandescence (PLII) measurement revealed that the soot level produced by the n-dodecane/m-xylene surrogate fuel is higher than that of the conventional jet fuel. For the combustion of fuels that do not contain aromatic compounds, the maximum local soot volume fraction (SVF) increases by a factor of approximately two when the ambient temperature rises from 900K to 1000K. On the other hand, the maximum SVF increases by a factor of at least five for the combustion of fuels which consist of aromatic volume of 23% to 27%. This corresponds with the reported experimental studies [19–22] where the sooting tendency of a single-component surrogate model is comparatively less significant than an alkane/aromatic mixture. Single component diesel surrogate models

which do not contain PAH chemistry in its original fuel composition are hence debatable since actual diesel fuels contain 20% to 30% of aromatic compounds [23].

Recognizing the limitation of single-component diesel surrogate fuel models, development of surrogate models with matching fuel compositions as the actual diesel fuels is necessary. Consequently, multi-component diesel surrogate models with blends of various fuel components have been proposed [7,24–30]. The details of the surrogate mechanisms, together with their respective constitutional components are provided in Table 1. In the earlier years, the number of components in a surrogate model was limited owing to the complexity in solving the stiff ordinary differential equations and the associated high computational cost. Besides, huge quantity of work was required to develop the database and mechanistic understanding of the surrogate components for diesel fuels [7]. Fuel blends which are commonly employed in numerical simulations of diesel combustion are Integrated Diesel European Action (IDEA) mechanism [27,28,31], Primary Reference Fuels (PRF) mechanism [32–35] and Diesel Oil Surrogate (DOS) mechanism [36]. With rapid advancement in chemical kinetics as well as computing power, surrogate models with greater number of fuel components are established such as PRF+1 mechanism [24] and Toluene Reference Fuel/PAH (TRF-PAH) mechanism [25]. Nonetheless, PRF, PRF+1 and TRF-PAH surrogate models are predominantly developed for homogeneous charge compression ignition (HCCI) applications. In these chemical models, n-heptane is mainly employed to represent the n-alkane component. Although the component mass fraction in these fuel blends can be adjusted to generate diesel surrogate models with different CN, the maximum boundary of the CN range is constrained by the CN of n-heptane. Thus, they are not suitable to be used as surrogate models for fuels with higher CN such as a paraffinic diesel reference fuel blend [37] with a CN of 80. More recently, POLIMI_Diesel_201 mechanism has been developed by Ranzi et al. [38] which consists of toluene, xylene, methylnaphthalene and n-alkanes up to

HXN. The mechanism was well validated in chemical kinetic simulations through comparison of the ignition delay (ID) predictions with experimental measurements of a binary diesel surrogate mixture under auto-ignition condition [39]. On the other hand, Chang et al. [29] have also formulated a diesel surrogate fuel model comprising toluene, n-decane, iso-octane and methylcyclohexane. These hydrocarbons are selected to represent the aromatics, straight-, branched- and cyclo-alkane components in the actual diesel fuels, respectively. The integrated mechanism was comprehensively validated against the experimental data for each fuel constituent and blends, as well as for practical diesel fuel under wide-ranging operating conditions. However, the performance of these two surrogate models [29,38] is yet to be tested in multi-dimensional CFD modelling studies.

Set against this background, this study aims to develop appropriate multi-component diesel surrogate models which account for both diesel fuel ignition and combustion across wider CN range of actual diesel fuels. The reduced models of surrogate components for diesel fuels including HXN, HMN, cyclohexane (CHX) and toluene generated in Part I are applied here. Two combinations of multi-component diesel surrogate models with different fuel compositions and components are developed and first validated in zero-dimensional (0-D) chemical kinetic simulations. The first model consists of straight- and branched-alkanes while the second consists of aromatics, straight-, branched- and cyclo-alkanes. The fidelity of the multi-component models is further appraised through the comparisons made between measurements of a constant volume combustion chamber and the numerical results of two-dimensional (2-D) CFD spray combustion simulations. The study also examines the performance of the surrogate models in predicting soot formation with and without the inclusion of aromatics/cyclo-alkane components.

## 2. Development and Validations of Multi-Component Diesel Surrogate Fuel Models

In this section, a sequential procedure is applied to formulate the multi-component diesel surrogate models, as illustrated in Fig. 1. The procedure is similar to the model construction scheme of Slavinskaya et al. [40]. Here, a 'reduced-then-combined' model construction strategy is employed where the reduced models for each of the fuel components are first derived from the respective detailed models and are subsequently combined together to generate the multi-component diesel surrogate models. As such, the reduced models for each of the components are constructed and may be used for other applications. This strategy also limits errors and complications generated from reducing the combined, detailed surrogate models with more than 3,500 species.

The target applications of this work focus on chemical composition match as well as mimicking the combustion and soot precursor formation behaviours of real diesel fuels such as #2 diesel fuel (D2). In this work, the reduced mechanism of HXN is designated as the base mechanism as it is the most abundant and largest hydrocarbon among the fuel constituents. Subsequently, the reduced mechanisms for other surrogate fuel components are added to the base mechanism to generate two combinations of multi-component diesel surrogate models:

(a) Multi-Component Diesel Surrogate No. 1 **(**MCDS1**)**: HXN + HMN;

(b) Multi-Component Diesel Surrogate No. 2 (MCDS2**)**: HXN + HMN + toluene + CHX.

The reduced mechanisms of HXN, HMN and CHX generated in Part I are employed. It is noted that the base chemistries of the fuel constituents are essentially similar as the reactions mechanisms are constructed based on the hierarchical nature of hydrocarbon–oxygen systems [9,41,42] in order to ensure that the results may not be affected when the based model is replaced by different models. The approach is similar to the model construction of the detailed mechanisms of n-heptane and iso-octane by Curran et al. [43,44].

The CN of MCDS1 is calculated using Equation (1):

147 $$\text{CN of mixture} = [F_{HXN} + 0.15F_{HMN}] \times 100 \quad (1)$$

148 $F_{HXN}$ is the mass fraction of HXN and $F_{HMN}$ is the mass fraction of HMN. The CN and
149 compositions of MCDS1 are determined based on those of Diesel Primary Reference Fuel
150 (DPRF58) [45]. DPRF58 is a fuel mixture of 42% HXN and 58% HMN by mass,
151 corresponding to a CN of 50.7. It was found to yield the same ID timings as the D2 fuel
152 experimentally [46,47]. However, Equation (1) is not applicable for fuel model which
153 considers other components. The compositions of MCDS2 are hence determined based on
154 those of the D2 fuel. The composition of toluene is fixed at 28% which is close to the
155 aromatic composition of D2 provided in the study by Kook and Pickett [48] and it is also
156 approximately the average value of the aromatic composition of typical North American
157 diesel fuels [7]. Subsequently, mass fractions of the remaining fuel components such as
158 HXN, HMN and CHX are iterated to match the IDs of D2. The properties of D2, MCDS1 and
159 MCDS2 surrogate models as well as size of the surrogate models are presented in Table 2.

160 Upon the construction of the multi-component diesel surrogate models, the relative
161 contribution of each reaction pathway to the net production rate of each species has altered as
162 compared with that of the respective single-component model. The reaction pathways of each
163 fuel species in the multi-component diesel surrogate mechanisms are hence reassessed using
164 reaction pathway analysis. It is observed that there are certain species which can be removed
165 from the mechanisms owing to their insignificant effect on the predictions of fuel oxidation
166 process upon integration. One of the examples of the eliminated species is the alkyl radical of
167 HMN, namely HMN-R1. It is formed mainly through H-atom abstraction and alkyl radical
168 decomposition from the fuel species. During the reduction of the detailed HMN mechanism,
169 two isomers of HMN are retained during chain-branching process such as HMN-R8 and
170 HMN-R1. However, when HMN is combined with other fuel components in the MCDS1 and
171 MCDS2 surrogate mechanisms, influence of HMN-R1 onto the formation of intermediate

species during chain branching process has become less significant. Therefore, HMN-R1, together with its corresponding reactions and connected species are removed from the mechanism. The species and reaction elimination process is performed in the following steps:

(i) Reaction path analysis is carried out for all test conditions. Here, the species for H2/CO and small hydrocarbon oxidations are not taken into consideration as these pools of species are shared by the fuel constituents in the integrated models. The normalised temperature *A*-factor sensitivities (as defined in Part I) for all reactions involving the potential eliminable species are calculated. If the sensitivity coefficient values for all the corresponding reactions are lower than the user-specified threshold value (i.e. 0.05) across all the test conditions, the species is then selected for the subsequent elimination procedure.

(ii) The model accuracy in ID and species profile predictions is selected as the criterion for the species elimination procedure upon model integration. Hence, the 0-D simulations across all the test conditions are repeated whenever a species is eliminated from the mechanism along with its corresponding elementary reactions so that the model predictions are not affected. The maximum relative error tolerance between the model predictions before and after elimination procedure is retained to within 5%. Sizes of the final, reduced multi-component diesel surrogate models are provided in Table 2.

Subsequently, mechanism validations in 0-D simulations are performed using the MCDS1 and MCDS2 diesel surrogate models for:

i) ID timing of each diesel fuel component (Fig. A1 in Appendix A);

ii) species concentration profiles of each diesel fuel component under auto-ignition (Fig. A2 in Appendix A) and JSR conditions (Fig. A3 in Appendix A);

iii) species concentration profiles of each diesel fuel component in a JSR (Fig. 2); and

iv) ID timing of DPRF58 [45] and n-dodecane (n-$C_{12}H_{26}$) [9]. (Fig. 3)

The test conditions applied here are described in part I. It is noteworthy that the computational results generated by both multi-component diesel models are plotted together with those predicted by each fuel constituent model. The purpose here is to demonstrate that the performance in predicting the ID timings and species concentrations retains after mechanism integration is carried out.

In Fig. A1, the computed IDs for HXN and HMN oxidations using MCDS1 and MCDS2 surrogate models are similar as the elementary reactions for HXN and HMN in these two mechanisms are the same. Comparison of ID timings and species profiles with those of CHX detailed mechanism is only performed using MCDS2 as MCDS1 does not contain elementary reactions for CHX. It is observed that the predicted ID timings for each surrogate model agree reasonably well with those of the surrogate components. In addition, trend of the species concentration profiles for both auto-ignition and JSR conditions is retained using both the multi-component surrogate models in comparison with those of each individual diesel fuel component, as shown in Fig. A2 and Fig. A3, respectively. The results for MCDS1 are comparable with those of MCDS2 with only about $\pm$5% deviations. Apart from that, the species concentration profiles in a JSR for each surrogate component are reproduced using the MCDS2 surrogate model. This is demonstrated in Fig. 2. The deviations in the species concentration predictions between the multi-component surrogate models and the individual detailed models for each fuel constituents can be attributed to the influence of kinetic reactions of other fuel components upon model integration. Despite the apparent difference in the absolute values, the relative trends of the species profiles computed by the detailed models are reasonably reproduced by the multi-component surrogate models.

Comparisons of the ID timing predictions between the surrogate models and DPRF58 are shown in Fig. 3(a). Agreement is achieved between the multi-component surrogate and DPRF58 mechanisms in ID predictions throughout the test conditions. Largest deviation is

observed for initial temperature of 850K and $\Phi$ of 1, which is recorded at 33%. The maximum deviations between the computations by the detailed and reduced models are successfully maintained to within an error tolerance of 40%, which is reasonable for large-scale mechanism reduction [51–54]. Apart from that, it is found that MCDS2 with compositions of $F_{HXN}$:$F_{HMN}$:$F_{C7H8}$:$F_{CHX}$ set to 0.42:0.20:0.28:0.10 yields similar ID timing predictions as DPRF58. In other words, its ignition behaviour is compatible with that of D2.

Moreover, the multi-component diesel surrogate mechanisms are further validated in closed homogeneous batch reactor simulations by varying their CN. ID timing predictions are compared in Fig. 3(b) with respect to the detailed n-dodecane mechanism (CN of 87). Composition of $F_{HXN}$:$F_{HMN}$ is set to 0.85:0.15 for MCDS1, corresponding to a CN of 87.25. On the other hand, the fuel composition for MCDS2 is fixed at 0.85:0.15:0:0 for $F_{HXN}$:$F_{HMN}$:$F_{C7H8}$:$F_{CHX}$. It is observed that the projected ID timings are well replicated using both MCDS1 and MCDS2 diesel surrogate models.

Upon the model validations under a series of different test conditions in the 0-D kinetic simulations, the proposed MCDS1 and MCDS2 surrogate models are coupled with CFD models in the next section to simulate spray combustion and soot formation under diesel-engine like conditions.

## 3. 2-D Spray Combustion Simulations

In this section, 2-D multi-dimensional CFD simulations are carried out to simulate spray combustion and soot formation processes using both the multi-component diesel surrogate fuel models. The spray combustion solver in OpenFOAM-2.0.x is used and a multistep soot model is integrated into the solver [55]. The numerical setups for the reacting diesel fuel sprays are described in Table 3(a). Further description of the numerical setups can be found in the former work [12,13]. In this work, the physical properties of the aromatic compounds

246 are represented by those of toluene. On the other hand, the physical properties of the alkanes
247 are represented by the physical properties of n-tetradecane as its physical properties are close
248 to those of real diesel fuels. Thus, the influence of fuel physical properties is isolated and the
249 effect of the chemical kinetics of reaction models can be studied.

250 Based on the sensitivity study shown in [56], the spatial and temporal evolutions of fourth
251 aromatic ring PAH, pyrene, are similar to those of smaller PAHs or $C_2H_2$ when the flame
252 temperature is relatively high (typically under no or low EGR conditions). Hence,
253 implementation of $C_2H_2$ as soot precursor is usually a good compromise between results
254 accuracy and simplicity when the PAH chemistry is absent [4,57–59]. $C_2H_2$ is selected as the
255 soot precursor in the numerical simulations using the MCDS1 surrogate model as this
256 mechanism does not contain PAH mechanism. On the other hand, $C_6H_6$ is present in the
257 MCDS2 surrogate model when CHX mechanism is integrated into the multi-component
258 mechanism during the model development stage. With the presence of the PAH chemistry in
259 the surrogate model, $C_6H_6$ is therefore designated as the soot precursor species in the
260 respective modelling studies. In order to simulate the mass addition on soot particle surface,
261 $C_2H_2$ is consistently used as the soot surface growth species when MCDS1 and MCDS2 are
262 applied. On the other hand, OH and $O_2$ are set as the soot oxidant species for the calculation
263 of soot mass destruction.

264 In this section, the numerical simulations are separated into two parts. First and foremost,
265 MCDS1 is applied in a sensitivity test to examine its reactivity towards variation in CN. Mass
266 fractions of HXN and HMN as well as the corresponding CN are shown in Table 3(b). It is
267 then followed by the validation of both MCDS1 and MCDS2 using the measurements of D2
268 fuel [18,48] from constant volume combustion chamber experiments. Mass fraction of each
269 component is varied to mimic the actual fuel properties, which are detailed in Table 2.
270 Operating conditions used for this validation exercise are demonstrated in Table 3(c).

Measurements are available for reacting spray test cases at 15% $O_2$ mole fraction. This condition represents a reactive environment of air diluted with exhaust gas recirculation. The ambient temperature varies from 900K to 1000K while the ambient density is fixed at 22.8kg/$m^3$. The computed ID, lift-off length (LOL) and SVF are compared to the experimental data. For the simulation results, ID is defined as the maximum dT/dt gradient of the temperature profile. On the other hand, LOL is defined as the distance from the injector to the closest layer where OH mass fraction reaches 2% of its maximum value in the domain. These definitions correspond with those recommended by Engine Combustion Network [50].

### *3.1 Sensitivity Test of the MCDS1 Surrogate Model on CN Variations*

The effects of variation in CN on LOL and ID predictions are demonstrated in Fig. 4(a). As the CN increases, it is expected that the ID becomes shorter. Thus, the ignition occurs at a location closer to the injection tip and the associated flame lift-off is hence shorter. The trend is replicated by the model. Based on the results shown in Fig. 4(a), it is observed that the kinetics of MCDS1 surrogate model is sensitive to changes in CN ranging from 15 to 100. MCDS1 serves as a promising surrogate model for diesel fuels with various CN.

In the next section, the MCDS1 model is further validated using the D2 fuel data. Its performance is also compared against that of the counterpart MCDS2 which considers CHX and toluene reactions.

### *3.2 Validation using D2 experimental data*

The predicted IDs and LOLs by MCDS1 and MCDS2 surrogate models for D2 fuel combustion at ambient temperatures of 900K and 1000K are demonstrated in Fig. 4(b). It is observed that the predictions follow the overall trend where the calculated ID and LOL decrease with increasing ambient temperature. The maximum deviations in ID and LOL

predictions with respect to the experimental measurements retain within 15.4% and 23%, respectively. The IDs calculated using MCDS1 agree well with the measurements in both cases but shorter LOLs are produced. On the other hand, the predicted IDs and LOLs are slightly longer in both cases when MCDS2 is applied. This can be attributed to the inclusion of toluene which is difficult to ignite. As it is considered in the initial composition of the MCDS2 model, the resulting ID becomes longer. The flame hence stabilises at a location further downstream from the injection tip, yielding a longer LOL. It is noted that the deviations between the experimental and computed LOLs using MCDS2 are less pronounced, where deviations of 3.5mm and 2.5mm are recorded for ambient temperatures of 900K and 1000K, respectively. It is worth mentioning that the deviations between the measured and computed LOLs can also be attributed to the absence of turbulence – chemistry interaction (TCI) in the numerical computations. Inclusion of TCI effects has been shown important to improve the prediction of the OH distributions and hence the development of flame lift-off [60–62].

In addition, the SVF predictions of D2 fuel using MCDS1 and MCDS2 are demonstrated in Fig. 5(a). The predictions are compared with the experimental soot clouds [18] obtained at quasi-steady state (4ms after start of injection) for ambient temperatures of 900K and 1000K. These experimental soot images are obtained from the PLII measurement which provides two-dimensional information of SVF distributions for D2 fuel. The red dashed lines on the images indicate the flame LOLs and only qualitative information of soot distribution in the fuel jets is provided based on the images obtained from the experiment. In Fig. 5(a), it is observed that the soot length predicted by MCDS2 is similar to that of the experimental measurements for D2 fuel combustion at ambient temperatures of 900K and 1000K. In contrast, the simulated soot clouds appear to be larger than the soot clouds observed in the experiments for both cases when MCDS1 is employed. In comparison to the predictions of

MCDS2, the soot clouds predicted by MCDS1 are formed at further upstream locations closer to the injection tip. This can be attributed to the associated shorter LOLs. Subsequently, quantitative SVF predictions along spray axis at quasi-steady state for D2 fuel combustion are demonstrated in Fig. 5(b). Results in Fig. 5(b) shows that the local SVF values produced by MCDS1 and MCDS2 are different. MCDS1 estimates maximum local SVF values of 15ppm and 24ppm for the 900K and 1000K test cases, respectively. On the other hand, the maximum local SVF values predicted by MCDS2 for the 900K and 1000K test cases are 5.8ppm and 12.2ppm, respectively. It is observed that the local SVF given by MCDS1 is consistently higher than that of MCDS2. This can be attributed to several reasons. First of all, the LOLs predicted by MCDS1 are shorter. The associated amount of air entrained into the fuel rich core region is lesser. Besides this, MCDS1 utilises $C_2H_2$ as soot precursor while MCDS2 uses $C_6H_6$. The mass concentration of $C_2H_2$ is commonly higher than that of PAH, leading to higher level of soot inception rate and hence soot mass gained. Lastly, as compared to MCDS1, the amount of branched-alkane (i.e. HMN) used in the initial fuel composition of the MCDS2 model is lower. As a consequence, the production rate of $C_2H_2$ drops and the soot mass gained through the soot surface growth process decreases correspondingly, yielding lower SVF values.

The next parameter used to evaluate the performance of the multi-component surrogate models is the soot formation behaviour at different ambient temperatures. The results indicates that the predicted maximum local SVF increases by a factor of 1.6 as the ambient temperature is raised from 900K to 1000K when MCDS1 is applied. The use of MCDS2 increases the maximum local SVF by a factor of 2.1. The ratio of increment in maximum SVF from ambient temperature of 900K to 1000K is henceforth represented by $ratio_{SVF}$ for brevity. Based on the measurement presented by Kook and Pickett [18], the experimental $ratio_{SVF}$ is more than three for D2 fuel combustion. The use of MCDS2 is found to improve

the overall simulated $ratio_{SVF}$. This can be attributed to the inclusion of aromatic and cyclo-alkane components in the initial fuel composition in MCDS2. At different ambient temperatures, the production of $C_2H_2$ is different when the aromatic and cyclo-alkane components are considered and omitted. This is further elaborated in the subsequent section.

Numerical analysis of $C_2H_2$ and $C_6H_6$ formations is performed at times when temperature rises by 100K, 200K, 400K, 800K and 1000K from the initial ambient temperatures. The results are demonstrated in Fig. 6 and the temperature tolerance for this comparison study is $\pm$20K. Besides these, $C_2H_2$ and $C_6H_6$ formations at quasi-steady state are also provided, in which the computed results are obtained at 4ms after the time of injection to ensure that the formation of the selected species in all test cases reaches a quasi-steady state. The observations obtained from the numerical analysis are discussed below:

(i) Results in Fig. 6(a) depict that the amount of $C_2H_2$ produced at the temperature rise of 100K from the initial ambient temperatures of 900K and 1000K is lower than $C_6H_6$ when both MCDS1 and MCDS2 are applied. $C_6H_6$ is mainly produced through the breakdowns of cyclo-paraffin ring as well as toluene via R1 to R4.

$$CYCHEXENE + OH \Leftrightarrow CYHX1N3J + H_2O \quad (R1)$$

$$CYHX13ENE + H \Leftrightarrow CYHX1N3J \quad (R2)$$

$$CYHX13ENE \Leftrightarrow C_6H_6 + H_2 \quad (R3)$$

$$C_6H_5CH_3 \Leftrightarrow C_6H_6 + CH_3 \quad (R4)$$

(ii) At temperature interval of 200K from the initial ambient temperatures, it is observed that the maximum values of $C_2H_2$ calculated using MCDS2 are approximately two-fold and five-fold greater than those predicted by MCDS1 in the 900K and 1000K cases, respectively. This is depicted in Fig. 6(b). The apparent differences in the predicted $C_2H_2$ levels can be attributed to the significant amount of $C_6H_6$ produced by MCDS2, which

subsequently leads to higher production rate of $C_2H_2$ as compared to that of MCDS1. The key formation pathways to $C_2H_2$ from $C_6H_6$ are described by reactions R5 to R7.

$$C_6H_6 \Leftrightarrow 2C_3H_3 \quad \text{(R5)}$$

$$C_3H_3 + H \Leftrightarrow C_3H_2 + H_2 \quad \text{(R6)}$$

$$C_3H_2 + OH \Leftrightarrow C_2H_2 + HCO \quad \text{(R7)}$$

(iii) In Fig. 6(c), it is observed that the peak mass fractions of $C_2H_2$ in the 1000K cases are consistently higher than those in the 900K cases when the initial ambient temperatures increase by 400K, disregards the use of MCDS1 and MCDS2. This is due to the higher production rate of $C_2H_2$ from the dissociation of $C_6H_6$ by R5 to R7 using MCDS2 as well as the consumption of $C_2H_4$ using both MCDS1 and MCDS2 in the 1000K cases. The formation of $C_2H_2$ is significantly dependent on $C_2H_4$ and the main formation pathways from $C_2H_4$ to $C_2H_2$ are described by reactions R8 to R10.

$$C_2H_4 + M \Leftrightarrow C_2H_2 + H_2 + M \quad \text{(R8)}$$

$$C_2H_4 + OH \Leftrightarrow C_2H_3 + H_2O \quad \text{(R9)}$$

$$C_2H_3 + M \Leftrightarrow C_2H_2 + H + M \quad \text{(R10)}$$

(iv) At temperature interval of 800K from the initial ambient temperatures, the associated mass fractions of $C_2H_2$ predicted by MCDS1 start to grow significantly and the peak values match with those produced by MCDS2, as demonstrated in Fig. 6(d). As discussed in the previous section, MCDS1 contains higher amount of branched-alkane in the initial fuel composition. As a result, the production rate of $C_2H_2$ becomes higher than that of MCDS2 which eventually results in the current observation.

(v) Same observation as of Fig. 6(d) persists until approaching ignition points.

(vi) The associated mass fractions of $C_2H_2$ continue to rise and eventually those predicted by MCDS1 become higher for both 900K and 1000K cases upon reaching a quasi-steady

state, as illustrated in Fig. 6(f). This corresponds well with the earlier findings in Fig. 5(b), in which SVF predictions by MCDS2 are lower for both 900K and 1000K cases.

The current results suggest that the MCDS1 model is useful for the soot formation simulations where the effect of aromatic chemistry plays a less significant role. For instance, Vishwanathan and Reitz [63] reasonably captured the variation of SVF with respect to the change of injection pressure and injector diameter using a single-component surrogate model, namely n-heptane, showing that the presence of aromatic compounds has less pronounced impact on such application. On the other hand, this work demonstrates that the overall soot formation predictions have been improved by considering cyclo-alkane and aromatic compounds. The revised counterpart, MCDS2, is found to predict a higher $ratio_{SVF}$ when the ambient temperature varies. Yet, the computed $ratio_{SVF}$ is under-predicted as compared to that of the experiment measurement where $ratio_{SVF} > 3$ is recorded. Further improvement is necessary on the coupled MCDS2-soot model to simulate the complex soot formation phenomenon.

The ambient pressure is increased to retain the ambient density of 22.8kg/m$^3$ as the ambient temperature varies between 900K and 1000K in the current test cases. However, the conventional multistep soot model does not capture pressure effects of soot formation [56]. The current soot model assumes that soot particles grow primarily by the addition of gaseous $C_2H_2$. The use of a pressure dependent surface growth model constant is expected to improve $ratio_{SVF}$. Alternatively, the inclusion of PAH condensation effects on soot formation under such high pressure, high temperature environment may aid to improve the prediction as well. Bisetti et al. [64] who implemented Hybrid Method of Moments in their Direct Numerical Simulation of soot formation in the n-heptane/air turbulent non-premixed flame revealed that PAH condensation is significant to the soot mass generation.

It is noteworthy that NOx submodel was not included in the multi-component diesel surrogate fuel models. Despite of this, these fuel models are expected to produce reasonable predictions for thermal NOx, which is the major portion of NOx emissions in conventional diesel engines. Thermal NOx formation rate is highly dependent on temperature [65], hence reasonable predictions of the temperature is the pre-requisite for the associated calculation. In the current numerical simulations, the maximum local temperatures calculated by the integrated fuel models are between 2300K and 2400K. These predictions are consistent with those obtained in the study of Pickett et al. [66] for 15% ambient oxygen. Apart from these, it is noteworthy that the accurate predictions of OH concentrations are essential for simulating thermal NOx formation. Based on the kinetic studies in the 0-D simulations (as shown in Fig. A2 and A3 in Appendix A), it is observed that the OH mole fractions predicted by the integrated models correspond reasonably well with the computations of the detailed models. However, it should also be highlighted that the computation of thermal NOx emissions also depends on the associated Arrhenius rate constants [67]. Hence, the surrogate models can be useful for thermal NOx simulations only when they are integrated with the extended Zeldovich reaction rates which are validated for engine applications.

## 4. Conclusions

In this study, two multi-component diesel surrogate models namely MCDS1 and MCDS2 with different fuel compositions and components have been introduced. MCDS1 model consists of straight- (HXN) and branched- (HMN) alkanes while MCDS2 consists of aromatic hydrocarbon (toluene), straight- (HXN), branched- (HMN) and cyclo- (CHX) alkanes. Surrogate fuel models with CN values ranging from 15 to 100 can be produced through blending of HXN and HMN. In addition, CHX and toluene are incorporated into MCDS2 model to achieve compositional match and to improve soot formation predictions. The integrated models are comprehensively validated in 0-D chemical kinetic simulations

under a wide range of shock tube and JSR conditions, by comparing the computations to those predicted by each detailed and reduced fuel constituent models. It is found that performance of the surrogate models in ID and species concentration predictions under both auto-ignition and JSR conditions is maintained after mechanism integration. Apart from these, the integrated models are also validated against the JSR experimental results for each diesel fuel constituents. Overall agreement between the computations and measurements is achieved with maximum deviations of one order of magnitude on the absolute values. Following that, the fidelity of both multi-component diesel surrogate models is further assessed in the 2-D spray combustion simulations. Numerical results reveal that MCDS1 is sensitive to the change of CN. The predicted ID and LOL correspond well with the variation of CN. Next, ID, LOL and SVF calculated using MCDS1 and MCDS2 are validated against constant volume combustion chamber experimental data. ID and LOL predictions given by both surrogate models agree reasonably well with the D2 measurements. Besides, it is observed that MCDS2 is able to provide better predictions in soot formation events than MCDS1 due to the inclusion of aromatic and cyclo-alkane components. It is revealed that $ratio_{SVF}$ of 1.6 is obtained for D2 fuel combustion when the ambient temperature increases from 900K to 1000K with the absence of aromatic and cyclo-alkane components. The simulated $ratio_{SVF}$ increases to 2.1 when both components are incorporated into the base mechanism as the inclusion of these two components provides alternative pathways to form rich species such as $C_2H_2$ and $C_6H_6$. In this work, the effects of including aromatic and cyclo-alkane components in the surrogate model on soot formation events are highlighted. It is demonstrated that MCDS2 is a potential surrogate model for D2 fuel. Nonetheless, additional work is required to improve the coupled MCDS2-soot model in simulating the complex soot formation phenomenon.

**Acknowledgements**

The Ministry of Higher Education Malaysia is acknowledged for the financial support towards this project under the Fundamental Research Grant Scheme (FRGS) F0014.54.02. The work at Technical University of Denmark is supported by Innovation Fund Denmark and MAN Diesel & Turbo A/S through the RADIADE project.

## References

[1] Som S, Aggarwal SK. Effects of Primary Breakup Modeling on Spray and Combustion Characteristics of Compression Ignition Engines. Combust Flame 2010;157:1179–93.

[2] Ma G, Tauzia X, Maiboom A. One-Dimensional Combustion Model with Detailed Chemistry for Transient Diesel Sprays. Proc Inst Mech Eng Part D: J Automob Eng 2014;228:457–76.

[3] Pang KM, Ng HK, Gan S. In-Cylinder Diesel Spray Combustion Simulations Using Parallel Computation: A Performance Benchmarking Study. Appl Energy 2012;93:466–78.

[4] Bolla M, Wright YM, Boulouchos K, Borghesi G, Mastorakos E. Soot Formation Modeling of n-Heptane Sprays Under Diesel Engine Conditions Using the Conditional Moment Closure Approach. Combust Sci Technol 2013;185:766–93.

[5] Pitsch H, Wan YP, Peters N. Numerical Investigation of Soot Formation and Oxidation Under Diesel Engine Conditions. SAE Tech Paper 952357; 1995.

[6] Singh S, Reitz RD, Musculus MPB. Comparison of the Characteristic Time (CTC), Representative Interactive Flamelet (RIF), and Direct Integration with Detailed Chemistry Combustion Models against Optical Diagnostic Data for Multi-Mode Combustion in a Heavy-Duty DI Diesel Engine. SAE Technical Paper 2006-01-0055; 2006.

[7] Farrell JT, Cernansky NP, Dryer FL, Law CK, Friend DG, Hergart CA, et al. Development of an Experimental Database and Kinetic Models for Surrogate Diesel Fuels. SAE Technical Paper 2007-01-0201; 2007.

[8] Sahetchian KA, Blin N, Rigny R, Seydi A, Murat M. The Oxidation of n-Butane and n-Heptane in a CFR Engine. Isomerization Reactions and Delay of Autoignition. Combust Flame 1990;79:242–9.

[9] Westbrook CK, Pitz WJ, Herbinet O, Curran HJ, Silke EJ. A Comprehensive Detailed Chemical Kinetic Reaction Mechanism for Combustion of n-Alkane Hydrocarbons from n-Octane to n-Hexadecane. Combust Flame 2009;156:181–99.

[10] Naik CV, Puduppakkam K, Meeks E, Liang L. Ignition Quality Tester Guided Improvements to Reaction Mechanisms for n-Alkanes: n-Heptane to n-Hexadecane. SAE Technical Paper 2012-01-0149; 2012.

[11] Ristori A, Dagaut P, Cathonnet M. The Oxidation of n-Hexadecane: Experimental and Detailed Kinetic Modeling. Combust Flame 2001;125:1128–37.

[12] Poon HM, Ng HK, Gan S, Pang KM, Schramm J. Evaluation and Development of Chemical Kinetic Mechanism Reduction Scheme for Biodiesel and Diesel Fuel Surrogates. SAE Int J Fuels Lubr 2013;6:729–44.

[13] Poon HM, Ng HK, Gan S, Pang KM, Schramm J. Development and Validation of Chemical Kinetic Mechanism Reduction Scheme for Large-Scale Mechanisms. SAE Int J Fuels Lubr 2014;7:653–62.

[14] Cowart JS, Fischer WP, Hamilton LJ, Caton PA, Sarathy SM, Pitz WJ. An Experimental and Modeling Study Investigating the Ignition Delay in a Military Diesel

Engine Running Hexadecane (Cetane) Fuel. Int J Engine Res 2012;14:57–67.
[15] Dryer FL, Ju Y, Brezinsky K, Santoro RJ, Litzinger TA, Sung C-J. Science-Based Design of Fuel-Flexible Chemical Propulsion/Energy: Generation of Comprehensive Surrogate Kinetic Models and Validation Databases for Simulating Large Molecular Weight Hydrocarbon Fuels. AF Office of Scientific Research Final Report, Grant No. FA9550-07-1-0515; 2012.
[16] Meijer M. Characterization of n-Heptane as a Single Component Diesel Surrogate Fuel. Technical University of Eindhoven Automotive Technology, Graduation Thesis; 2010.
[17] Galle J, Sebastian V. Influence of Diesel Surrogates on the Behavior of Simplified Spray Models. Proc FISITA 2012 World Automot Congr 2013;189:361–74.
[18] Kook S, Pickett LM. Soot Volume Fraction and Morphology of Conventional, Fischer-Tropsch, Coal-Derived, and Surrogate Fuel at Diesel Conditions. SAE Int J Fuels Lubr 2012;5:647–64.
[19] Lemaire R, Faccinetto A, Therssen E, Ziskind M, Focsa C, Desgroux P. Experimental Comparison of Soot Formation in Turbulent Flames of Diesel and Surrogate Diesel Fuels. Proc Combust Inst 2009;32 I:737–44.
[20] Barths H, Pitsch H, Peters N. 3D Simulation of DI Diesel Combustion and Pollutant Formation Using a Two-Component Reference Fuel. Oil Gas Sci Technol 1999;54:233–44.
[21] Dagaut P, Cathonnet M. The Ignition, Oxidation, and Combustion of Kerosene: A Review of Experimental and Kinetic Modeling. Prog Energy Combust Sci 2006;32:48–92.
[22] Mathieu O, Djebaïli-Chaumeix N, Paillard CE, Douce F. Experimental Study of Soot Formation from a Diesel Fuel Surrogate in a Shock Tube. Combust Flame 2009;156:1576–86.
[23] Pitz WJ, Mueller CJ. Recent Progress in the Development of Diesel Surrogate Fuels. Prog Energy Combust Sci 2011;37:330–50.
[24] Chaos M, Zhao Z, Kazakov A, Gokulakrishnan P, Angioletti M, Dryer FL. A PRF + Toluene Surrogate Fuel Model for Simulating Gasoline Kinetics. In: 5th US Combust Meet 2007:1–19.
[25] Wang H, Jiao Q, Yao M, Yang B, Qiu L, Reitz RD. Development of an n-Heptane/Toluene/Polyaromatic Hydrocarbon Mechanism and Its Application for Combustion and Soot Prediction. Int J Engine Res 2013;14:434–51.
[26] Westbrook CK, Pitz WJ, Mehl M, Curran HJ. Detailed Chemical Kinetic Reaction Mechanisms for Primary Reference Fuels for Diesel Cetane Number and Spark-Ignition Octane Number. Proc Combust Inst 2011;33:185–92.
[27] Schindler K. Intregrated Diesel European Action ( IDEA ): Study of Diesel Combustion. SAE Technical Paper 920591; 1992.
[28] Hentschel W, Schindler K, Haahtela O. European Diesel Research IDEA-Experimental Results from DI Diesel Engine Investigations. SAE Technical Paper 941954; 1994.
[29] Chang Y, Jia M, Li Y, Liu Y, Xie M, Wang H, et al. Development of a Skeletal Mechanism for Diesel Surrogate Fuel by Using a Decoupling Methodology. Combust Flame 2015;162:3785–802.
[30] Frassoldati A, D'Errico G, Lucchini T, Stagni A, Cuoci A, Faravelli T, et al. Reduced Kinetic Mechanisms of Diesel Fuel Surrogate for Engine CFD Simulations. Combust Flame 2015;162:3991–4007.
[31] Hergart C, Barths H, Peters N. Modeling the Combustion in a Small-Bore Diesel Engine Using a Method Based on Representative Interactive Flamelets. SAE Technical Paper 1999-01-3550; 1999.

561 [32] Curran H, Pitz W, Westbrook C, Callahan CV, Dryer FL. Oxidation of Automotive
562 Primary Reference Fuels at Elevated Pressures. Proc Combust Inst 1998;27:379–87.
563 [33] Kirchen P, Shahbakhti M, Koch CR. A Skeletal Kinetic Mechanism for PRF
564 Combustion in HCCI Engines. Combust Sci Technol 2007;179:1059–83.
565 [34] Wang H, Yao M, Reitz RD. Development of a Reduced Primary Reference Fuel
566 Mechanism for Internal Combustion Engine Combustion Simulations. Energy & Fuels
567 2013;27:7843–53.
568 [35] Lawrence Livermore National Laboratory Physical and Life Sciences Directorate.
569 Available from: https://combustion.llnl.gov/archived-mechanisms/surrogates/prf-
570 isooctane-n-heptane-mixture.
571 [36] Golovitchev VI, Bergman M, Montorsi L. CFD Modeling of Diesel Oil and DME
572 Performance in a Two-Stroke Free Piston Engine. Combust Sci Technol
573 2007;179:417–36.
574 [37] Pickett LM, Siebers DL. Fuel Effects on Soot Processes of Fuel Jets at DI Diesel
575 Conditions. SAE Technical Paper 2003-01-3080; 2003.
576 [38] Ranzi E, Frassoldati A, Stagni A, Pelucchi M, Cuoci A, Faravelli T. Reduced Kinetic
577 Schemes of Complex Reaction Systems: Fossil and Biomass-Derived Transportation
578 Fuels. Int J Chem Kinet 2014;46:512–42.
579 [39] Wang H, Warner SJ, Oehlschlaeger MA, Bounaceur R, Biet J, Glaude PA, et al. An
580 Experimental and Kinetic Modeling Study of the Autoignition of α-
581 Methylnaphthalene/Air and α-Methylnaphthalene/n-Decane/Air Mixtures at Elevated
582 Pressures. Combust Flame 2010;157:1976–88.
583 [40] Slavinskaya N, Zizin A, Riedel U. Towards Kerosene Reaction Model Development:
584 Propylcyclohexane, cyC9H18, n-Dodecane, C12H26, and Hexadecane C16H34
585 combustion. AIAA 2010:1–13.
586 [41] Oehlschlaeger MA, Steinberg J, Westbrook CK, Pitz WJ. The Autoignition of iso-
587 Cetane at High to Moderate Temperatures and Elevated Pressures: Shock Tube
588 Experiments and Kinetic Modeling. Combust Flame 2009;156:2165–72.
589 [42] Silke EJ, Pitz WJ, Westbrook CK, Ribaucour M. Detailed Chemical Kinetic Modeling
590 of Cyclohexane Oxidation. J Phys Chem A 2007;111:3761–75.
591 [43] Curran HJ, Gaffuri P, Pitz WJ, Westbrook CK. A Comprehensive Modeling Study of
592 n-Heptane Oxidation. Combust Flame 1998;114:149–77.
593 [44] Curran HJ, Gaffuri P, Pitz WJ, Westbrook CK. A comprehensive Modeling Study of
594 iso-Octane Oxidation. Combust Flame 2002;129:253–80.
595 [45] Perini F, Sahoo D, Miles P, Reitz R. Modeling the Ignitability of a Pilot Injection for a
596 Diesel Primary Reference Fuel: Impact of Injection Pressure, Ambient Temperature
597 and Injected Mass. SAE Int J Fuels Lubr 2014:48–64.
598 [46] Sahoo D, Petersen B, Miles P. Measurement of Equivalence Ratio in a Light-Duty
599 Low Temperature Combustion Diesel Engine by Planar Laser Induced Fluorescence of
600 a Fuel Tracer. SAE Int J Engines 2011;4:2312–25.
601 [47] Petersen B, Miles PC, Sahoo D. Equivalence Ratio Distributions in a Light-Duty
602 Diesel Engine Operating Under Partially Premixed Conditions. SAE Int J Engines
603 2012;5:526–37.
604 [48] Kook S, Pickett LM. Liquid Length and Vapor Penetration of Conventional, Fischer–
605 Tropsch, Coal-Derived, and Surrogate Fuel Sprays at High-Temperature and High-
606 Pressure Ambient Conditions. Fuel 2012;93:539–48.
607 [49] Yaws CL. Thermophysical Properties of Chemicals and Hydrocarbons. Elsevier; 2009.
608 [50] Engine Combustion Network Experimental Data Archive. Available from:
609 http://www.sandia.gov/ecn/.
610 [51] Brakora JL, Ra Y, Reitz RD. Combustion Model for Biodiesel-Fueled Engine

Simulations Using Realistic Chemistry and Physical Properties. SAE Int J Engines 2011;4:931–47.
[52] Niemeyer KE, Sung C-J, Raju MP. Skeletal Mechanism Generation for Surrogate Fuels Using Directed Relation Graph with Error Propagation and Sensitivity Analysis. Combust Flame 2010;157:1760–70.
[53] Yang J, Johansson M, Naik C, Puduppakkam K, Golovitchev V, Meeks E. 3D CFD Modeling of a Biodiesel-Fueled Diesel Engine Based on a Detailed Chemical Mechanism. SAE Technical Paper 2012-01-0151; 2012.
[54] Luo Z, Plomer M, Lu T, Som S, Longman DE, Sarathy SM, et al. A Reduced Mechanism for Biodiesel Surrogates for Compression Ignition Engine Applications. Fuel 2012;99:143–53.
[55] Leung KM, Lindstedt RP, Jones WP. A Simplified Reaction Mechanism for Soot Formation in Nonpremixed Flames. Combust Flame 1991;87:289–305.
[56] Pang KM, Jangi M, Bai X-S, Schramm J. Evaluation and Optimisation of Phenomenological Multi-Step Soot Model for Spray Combustion Under Diesel Engine-Like Operating Conditions. Combust Theory Model 2015:1–30.
[57] Jangi M, Lucchini T, D'Errico G, Bai X-S. Effects of EGR on the Structure and Emissions of Diesel Combustion. Proc Combust Inst 2013;34:3091–8.
[58] Pang KM, Jangi M, Bai X-S, Schramm J. Investigation of Chemical Kinetics on Soot Formation Event of n-Heptane Spray Combustion. SAE Technical Paper 2014-01-1254; 2014.
[59] Kong S-C, Sun Y, Rietz RD. Modeling Diesel Spray Flame Liftoff, Sooting Tendency, and NO[sub x] Emissions Using Detailed Chemistry with Phenomenological Soot Model. J Eng Gas Turbines Power 2007;129:245–51.
[60] D'Errico G, Lucchini T, Contino F, Jangi M, Bai X-S. Comparison of Well-Mixed and Multiple Representative Interactive Flamelet Approaches for Diesel Spray Combustion Modelling. Combust Theory Model 2014;18:65–88.
[61] Bhattacharjee S, Haworth DC. Simulations of Transient n-Heptane and n-Dodecane Spray Flames Under Engine-Relevant Conditions Using a Transported PDF Method. Combust Flame 2013;160:2083–102.
[62] Pei Y, Hawkes ER, Kook S. A Comprehensive Study of Effects of Mixing and Chemical Kinetic Models on Predictions of n-Heptane Jet Ignitions with the PDF Method. Flow, Turbul Combust 2013;91:249–80.
[63] Vishwanathan G, Reitz RD. Development of a Practical Soot Modeling Approach and Its Application to Low-Temperature Diesel Combustion. Combust Sci Technol 2010;182:1050–82.
[64] Bisetti F, Blanquart G, Mueller ME, Pitsch H. On the Formation and Early Evolution of Soot in Turbulent Nonpremixed Flames. Combust Flame 2012;159:317–35.
[65] Christensen M, Hultqvist A, Johansson B. Demonstrating the Multi Fuel Capability of a Homogeneous Charge Compression Ignition Engine with Variable Compression Ratio. SAE Technical Paper 1999–01–3679; 1999.
[66] Pickett L, Siebers D, Idicheria C. Relationship Between Ignition Processes and the Lift-Off Length of Diesel Fuel Jets. SAE Technical Paper 2005-01-3843; 2005.
[67] Hernández JJ, Pérez-Collado J, Sanz-Argent J. Role of the Chemical Kinetics on Modeling NOx Emissions in Diesel Engines. Energy & Fuels 2008;22:262–72.

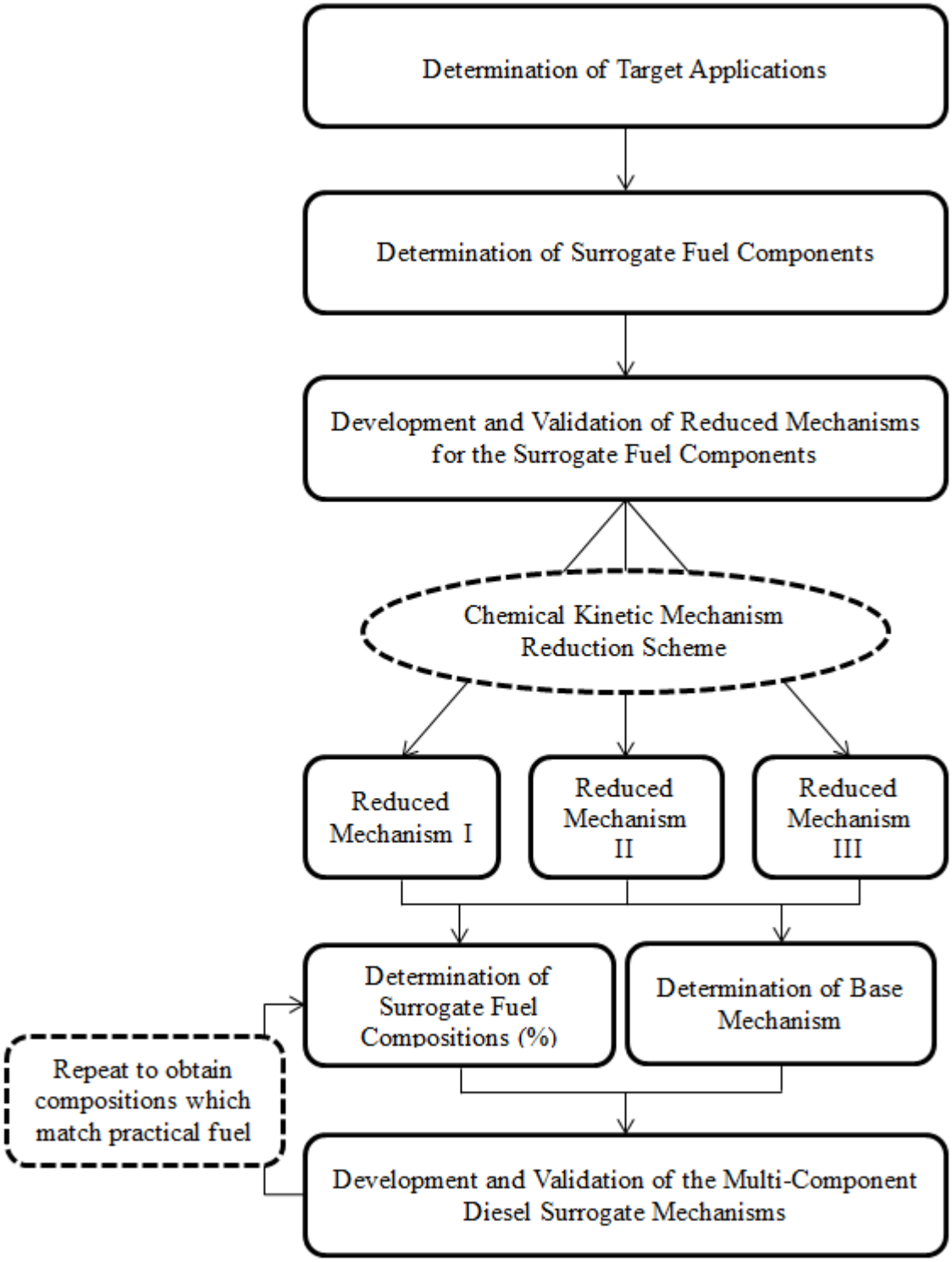


**Fig. 1 Sequential steps to formulate the multi-component diesel surrogate fuel models.**

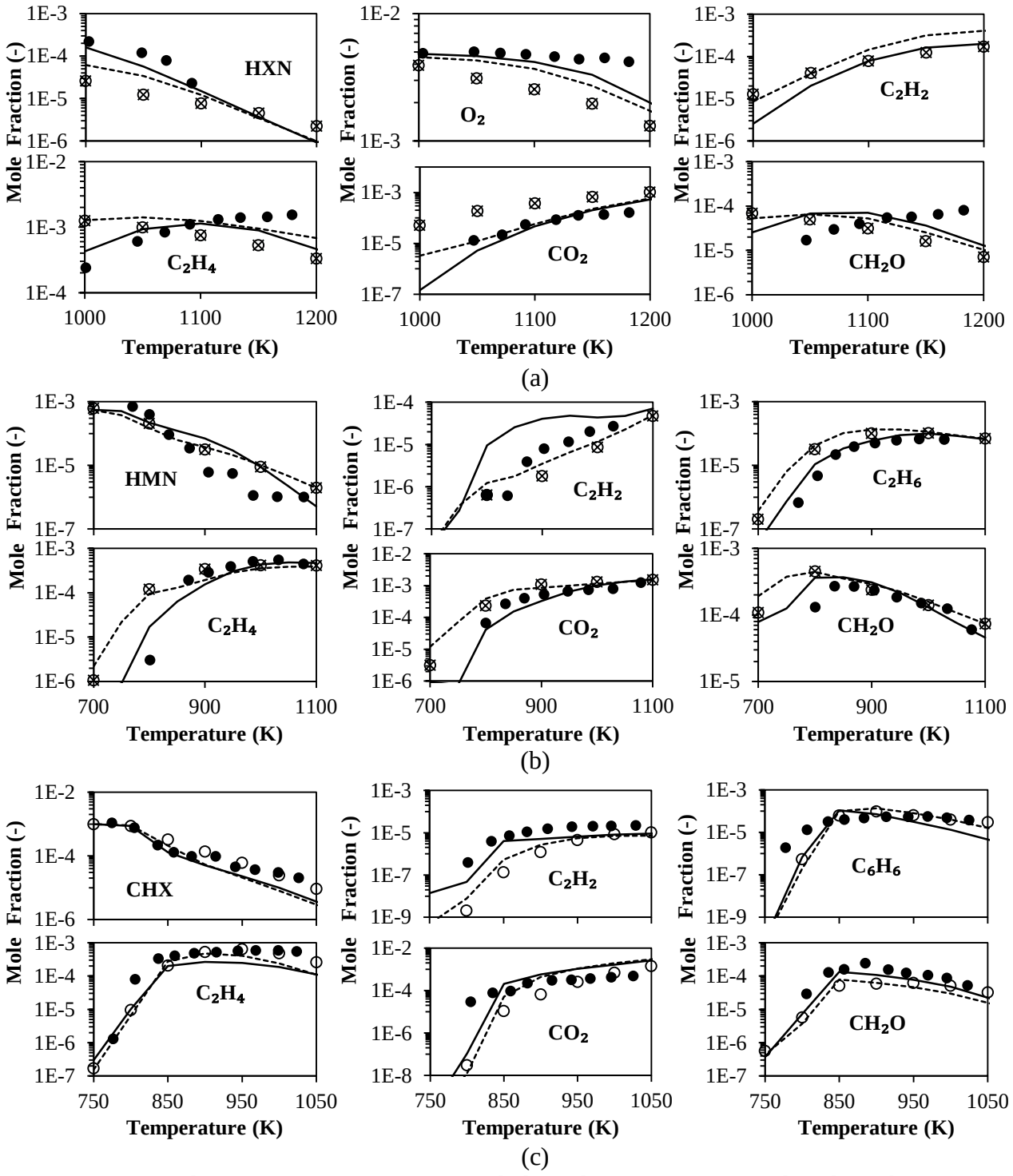


**Fig. 2 Computed and experimental species mole fractions obtained from the oxidation of (a) 0.03% HXN (pressure = 1atm, $\Phi$ = 1.5, residence time = 70ms), (b) 0.07% HMN (pressure = 10atm, $\Phi$ = 2, residence time = 1s), and (c) 0.1% CHX (pressure = 10atm, $\Phi$ = 1.5, residence time = 0.5s) under JSR conditions.**

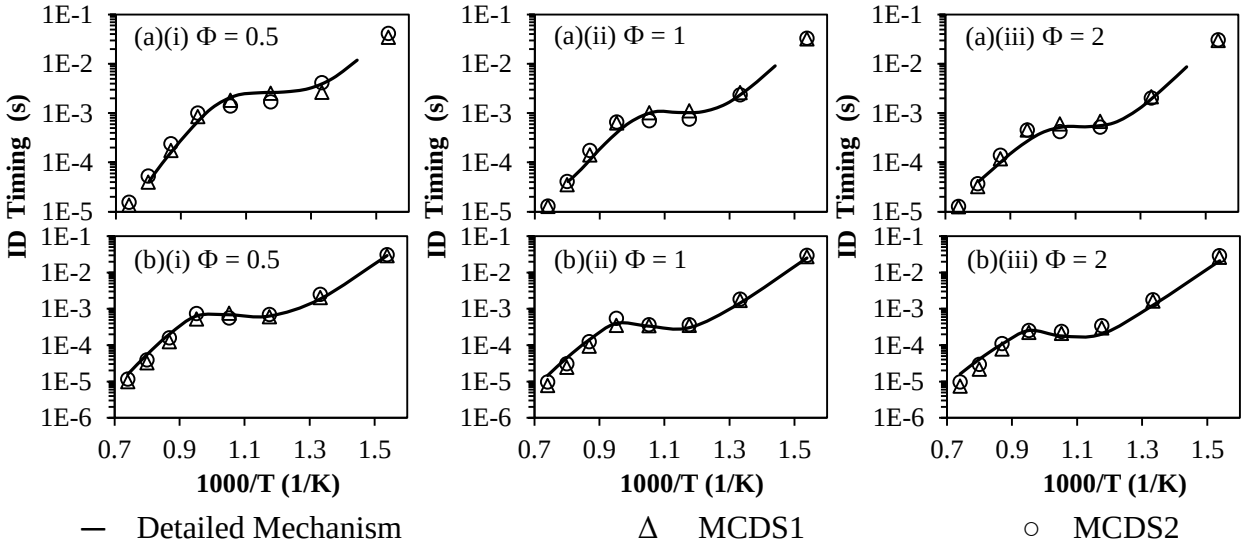


**Fig. 3 Comparisons of the ID predicted by MCDS1 and MCDS2 surrogate models with the detailed mechanisms of (a) DPRF58[a] [45] and (b) n-dodecane[b] [9] for initial pressure of 40bar, $\Phi$ of (i) 0.5, (ii) 1 and (iii) 2. [[a]IDs of DPRF58 were computed by Perini et al. [45] using the detailed mechanism of Westbrook et al. [26] in a constant volume vessel using identical initial conditions; [b]The mechanism of n-dodecane was extracted from the detailed mechanism of Westbrook et al. [9] for combustion of n-alkane hydrocarbons from n-octane to HXN.]**

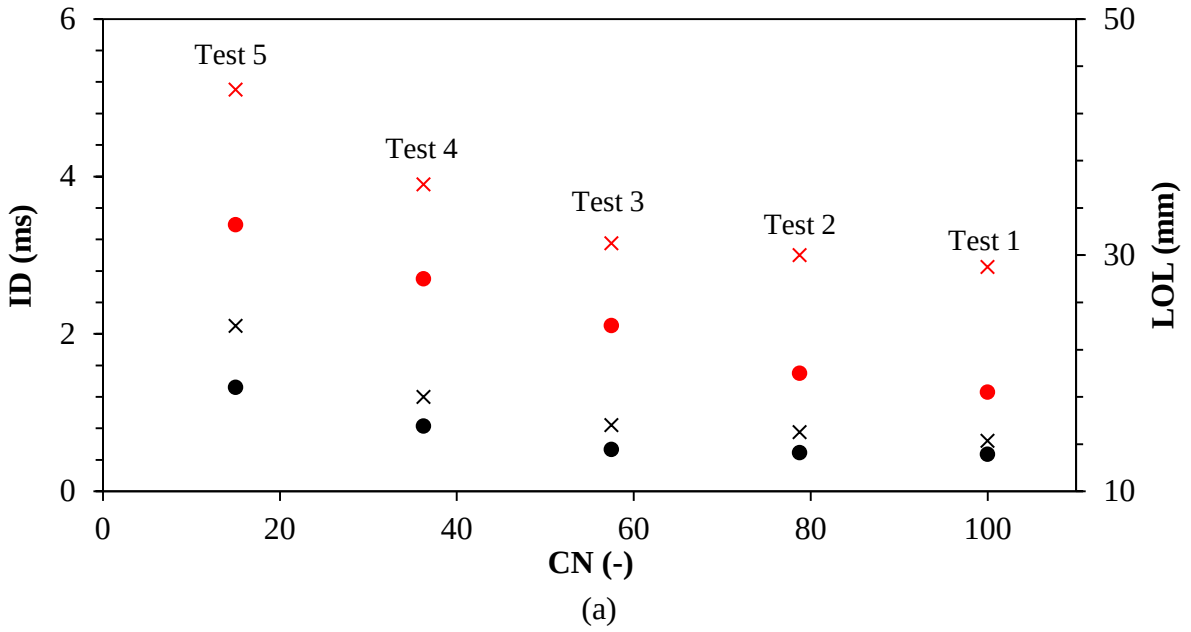


(a)

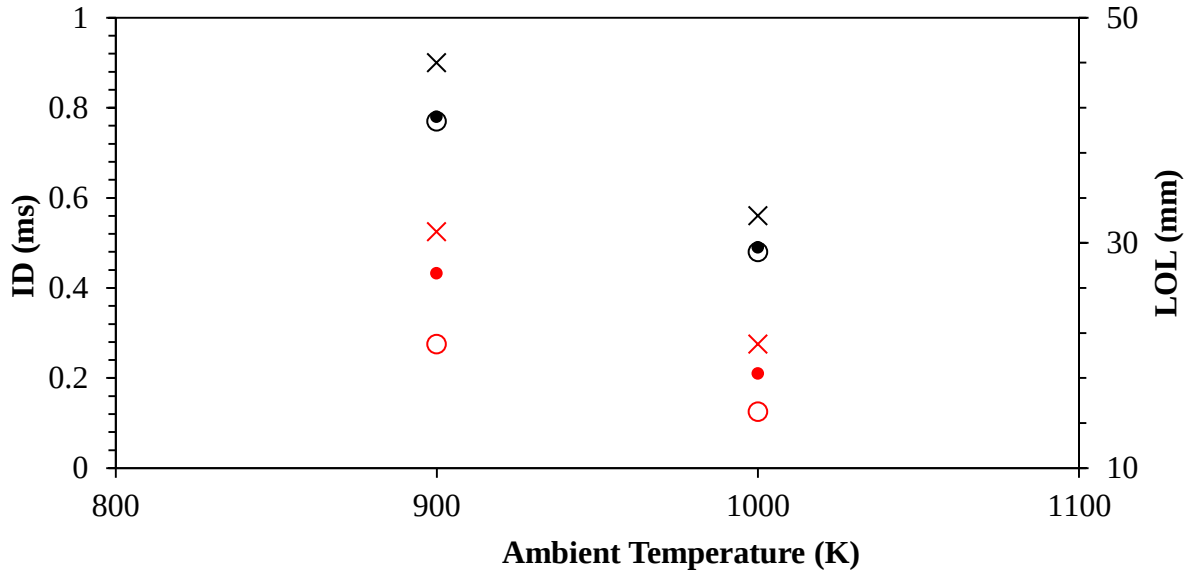


(b)

**Fig. 4 (a) ID (black) and LOL (red) predictions against CN for the sensitivity tests using MCDS1 surrogate model for ambient temperatures of 900K (X) and 1000K (●); (b) ID (black) and LOL (red) predictions using MCDS1 (○) and MCDS2 (X) surrogate models in comparison with the experimental measurements (●) for D2 fuel combustion for ambient temperatures of 900K and 1000K.**

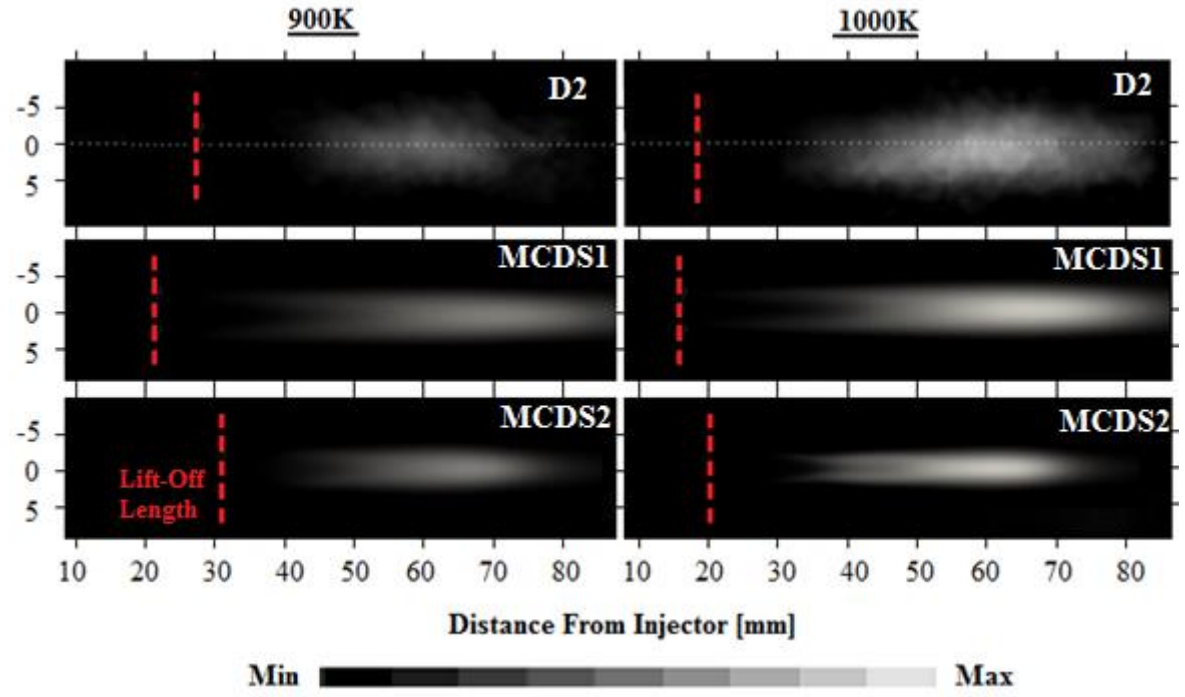


(a)

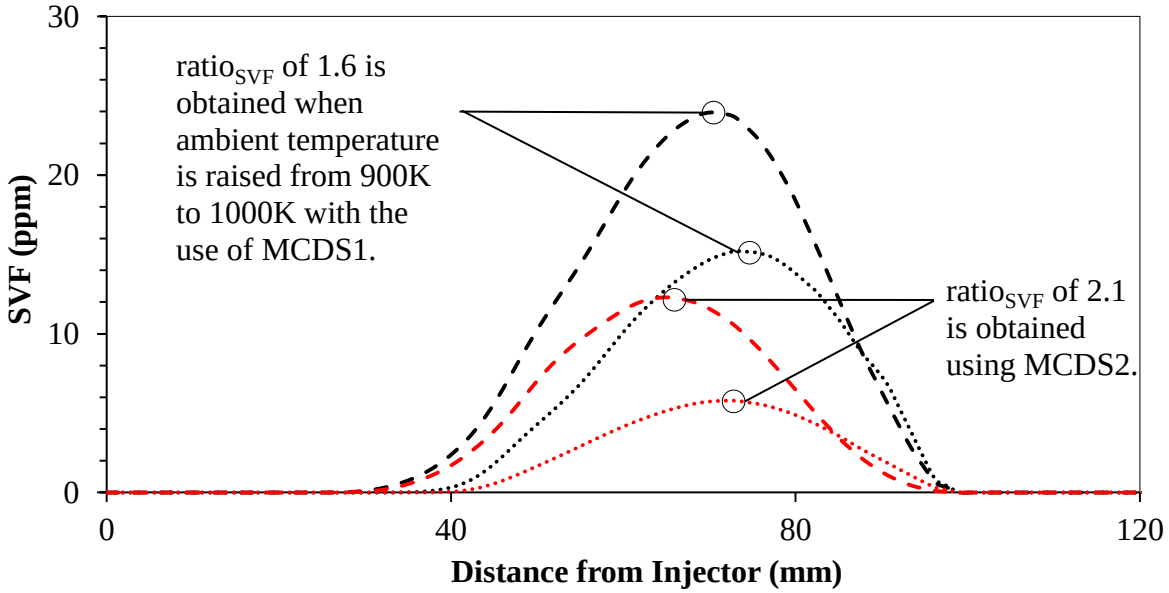


(b)

**Fig. 5 (a) Qualitative comparisons of predicted SVF contours and experimental soot cloud images at quasi-steady state for D2 fuel combustion in a constant volume chamber using MCDS1 and MCDS2 surrogate models; (b) Comparisons of the computed SVF along spray axis using MCDS1 (black) and MCDS2 (red) surrogate models at ambient temperatures of 900K (···) and 1000K (−−).**

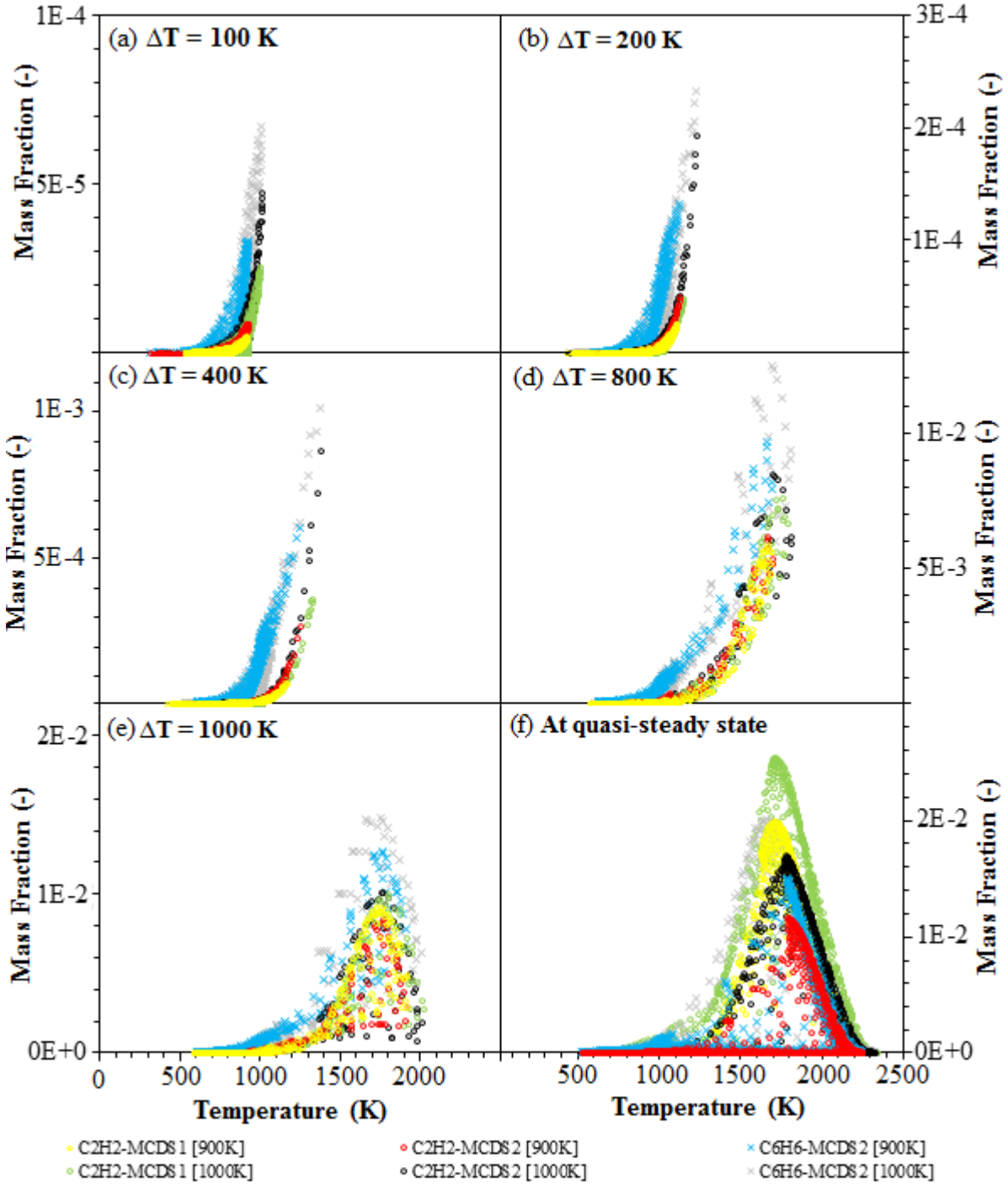


**Fig. 6 Comparisons of $C_2H_2$ and $C_6H_6$ mass fractions at temperature intervals of (a) 100K, (b) 200K, (c) 400K, (d) 800K, (e) 1000K and at (f) quasi-steady state for D2 fuel combustion at ambient temperatures of 900K and 1000K using MCDS1 and MCDS2 diesel surrogate models. [**Note: Mass fractions of $C_6H_6$ at ΔT = 100K, ΔT = 200K and ΔT = 400K are scaled down by a factor of 20, 10 and 5, respectively.]**

**Table 1 Details of the currently available multi-component surrogate fuel models.**

| Surrogate Models | Compositions | $N_S$ | $N_R$ | Model Descriptions | Year of Publication | Author(s) | Ref. |
|---|---|---|---|---|---|---|---|
| IDEA | n-decane, 1-methylnaphthalene | 118 | 557 | Describe fuel oxidation, soot and NOx formations; Contain low-temperature kinetics for auto-ignition. | 1999 | Hergart et al. | [31] |
| PRF | iso-octane, n-heptane | 990 | 4,060 | Describe auto-ignition and intermediate product formation at high-pressure conditions; Contain kinetic reactions for low to high temperatures as well as NTC behaviour. | 1998 | Curran et al. | [32] |
| | | 58 | 120 | Describe ignition of PRF in a HCCI engine; Contain kinetic reactions for intermediate and high temperatures. | 2007 | Kirchen et al. | [33] |
| | | 73 | 296 | Describe oxidation of diesel/gasoline; Contain kinetic reactions for low to high temperatures as well as NTC behaviour. Reduced model of Wang et al. [34] is developed based on the LLNL detailed model [35] . | 2013 | Wang et al. | [34] |
| | | 1,034 | 4,236 | | - | LLNL | [35] |
| Diesel PRF | HXN, HMN | 2,800 | 11,000 | Contain alkylperoxy radical sub-mechanism and kinetic reactions for low to high temperatures as well as NTC behaviour. | 2011 | Westbrook et al. | [26] |
| DOS | n-heptane, toluene | 70 | 305 | Describe fuel oxidation, soot and NOx formations; Optimised for engine applications. | 2007 | Golovitchev et al. | [36] |
| PRF+1 | iso-octane, n-heptane, toluene | 469 | 1,221 | Describe fuel oxidation and soot formations; Contain kinetic reactions for low and intermediate temperatures. | 2007 | Chaos et al. | [24] |
| TRF-PAH | n-heptane, toluene, PAH | 71 | 360 | Describe combustion and PAH formation; Contain kinetic reactions for low to high temperatures. | 2013 | Wang et al. | [25] |
| POLIMI_ Diesel_201 | HXN , toluene, xylene, methylnaphthalene | 201 | 4,240 | Validated under shock-tube (intermediate to high temperatures) and JSR (low to intermediate temperatures) simulations. | 2014 | Ranzi et al. | [38] |
| POLIMI_NC12 _96 + PAH | n-dodecane, PAH | 133 | 2,275 | Contain kinetic reactions for low to high temperatures; Reasonably capture the important characteristics of spray ignition processes. | 2015 | Frassoldati et al. | [30] |
| Skeletal Diesel Surrogate Fuel Model | n-decane, iso-octane, methylcyclohexane, toluene | 70 | 220 | Validated under shock-tube, JSR, flow reactor and pre-mixed laminar flame simulations. | 2015 | Chang et al. | [29] |

$N_S$ and $N_R$ denote the number of species and reactions, respectively; NTC is defined as negative temperature coefficient.

**Table 2 Fuel properties [18,48-50] and chemistry sizes of detailed/reduced chemical mechanism models used in the current work.**

| Properties | D2 | MCDS1 | MCDS2 |
|---|---|---|---|
| Chemical Formula (mass fraction) | $C_3$-$C_{25}$ | $F_{HXN}$ : $F_{HMN}$ = 0.42 : 0.58 | $F_{HXN}$ : $F_{HMN}$ : $F_{toluene}$ : $F_{CHX}$ = 0.42 : 0.20 : 0.28 : 0.10 |
| Type of Hydrocarbon | 33.8%[a] / 27%[b] Aromatics, 65.0%[a] Alkanes, 1.2%[a] Olefins | Straight- and branched-alkanes | Straight-, branched- and cyclo-alkanes, aromatic |
| CN | 46 (40-56) | 50.7 | - |
| Molecular Weight [g/mol] | ~200.000 | 226.446 | 174.612 |
| H/C Ratio | 1.800 | 2.125 | 1.838 |
| Lower Heating Value [MJ/kg] | 42.975 | 43.900[c] | 42.928[c] |
| Boiling Point [$^o$C] | 350 | 287 | 287 |
| Flash Point [$^o$C] | 73.0 | 111.5[c] | 74.7[c] |
| Size of final reduced mechanism ($N_S$; $N_R$) | - | 128; 408[d]<br>88; 284[e] | 169; 545[d]<br>129; 411[e] |

F denotes mass fraction

[a]Composition of aromatic compounds provided in the study of Pickett and Siebers [37]

[b]Composition of aromatic compounds provided in the study of Kook and Pickett [48]

[c]Volume-averaged properties are given for MCDS1 and MCDS2

[d]Before elimination of unimportant species and reactions upon integration

[e]After elimination of unimportant species and reactions upon integration

**Table 3 (a) CFD model setups used for reacting diesel fuel spray simulations; (b) Sensitivity test with various CN using MCDS1 surrogate model; (c) Experimental operating conditions.**

| **(a) Numerical Setups** | |
|---|---|
| Grid | Grading; 0.25mm x 0.25mm (minimum), 4mm x 2mm (maximum) in both radial and axial directions |
| Turbulence Model | Standard *k*-$\varepsilon$ ($C_\mu$ = 0.09 ; $C_1$ = 1.54 ; $C_2$ = 1.92 ; $C_3$ = -0.33 ; $\sigma_k$ = 1 ; $\sigma_\epsilon$ = 1.3) |
| Breakup Model | Reitz Diwakar ($C_{bag}$ = 6; $C_b$ = 0.785; $C_{strip}$ = 0.5; $C_s$ = 12) |
| Soot Model | Multi-step [55] |
| Time Step (s) | 5.00E-07 |
| Number of Parcels | 100,000 |
| Initial k ($m^2/s^2$) | 0.735 |
| Initial ε ($m^2/s^3$) | 3.5 |

| **(b) Sensitivity Test with Various CN** | | |
|---|---|---|
| **Tests** | **Compositions ($F_{HXN}$:$F_{HMN}$)** | **CN** |
| 1 | 1:0 | 100 |
| 2 | 0.75:0.25 | 78.75 |
| 3 | 0.50:0.50 | 57.5 |
| 4 | 0.25:0.75 | 36.25 |
| 5 | 0:1 | 15 |

| **(c) Experimental Operating Conditions** | |
|---|---|
| Ambient temperature (K) | 900/1000 |
| Ambient density ($kg/m^3$) | 22.8 |
| Ambient Pressure (MPa) | 6/6.7 |
| Orifice diameter (mm) | 0.09 |
| Ambient composition (%) | $O_2$ = 15%; $CO_2$ = 6.23%; $H_2O$ = 3.62%; $N_2$ = 75.15% |
| Injection duration (ms) | 7 |

*k* and $\varepsilon$ denote the turbulence kinetic energy and turbulence dissipation rate, respectively

**Appendix A: Validation Results for 0-D Chemical Kinetic Simulations**

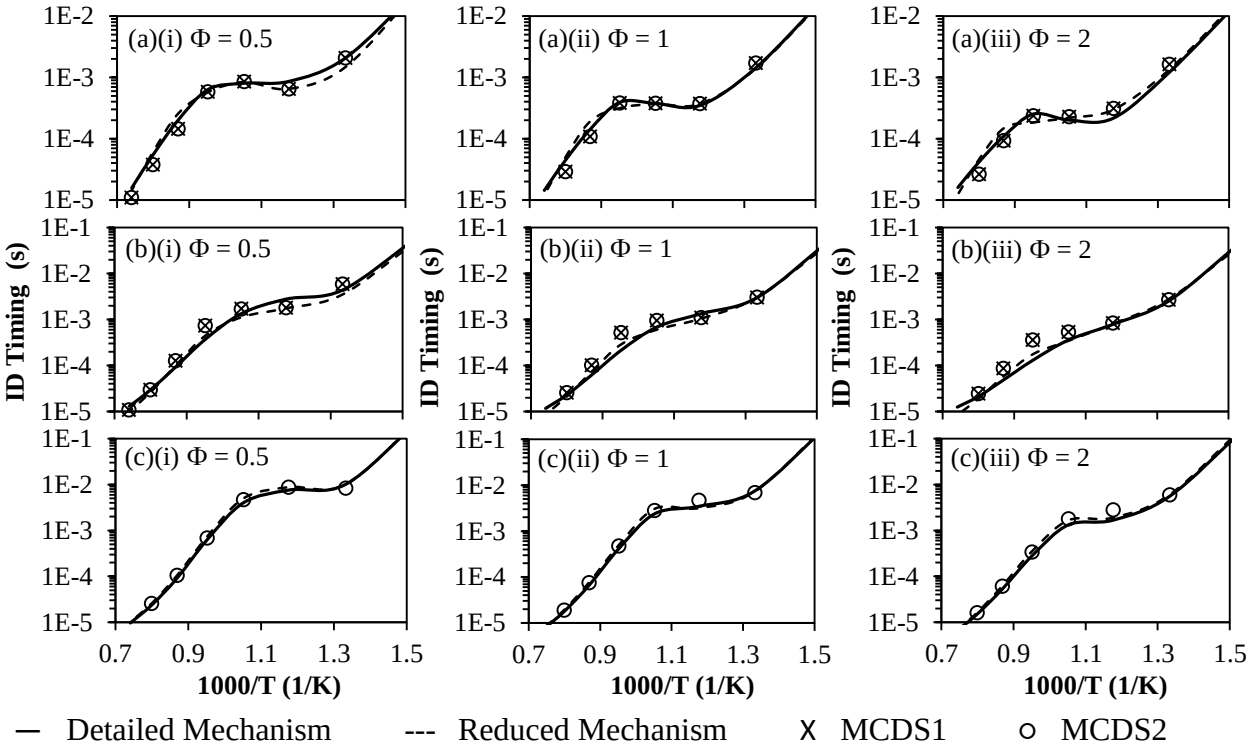


**Fig. A1 Computed ID of (a) HXN, (b) HMN and (c) CHX calculated by respective detailed and reduced mechanisms as well as MCDS1 and MCDS2 surrogate models, with initial pressure of 60bar and $\Phi$ of (i) 0.5, (ii) 1.0, (iii) 2.0.**

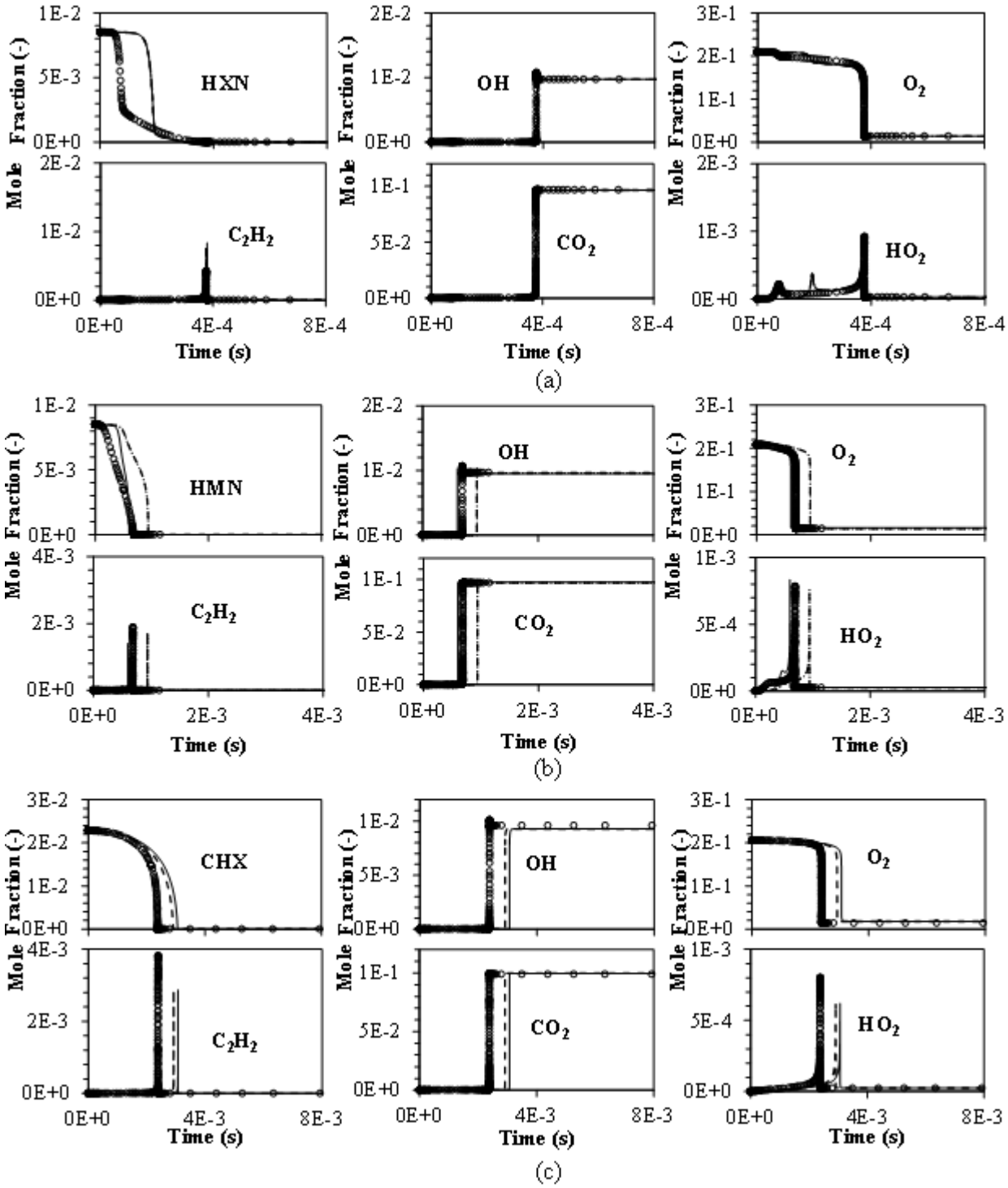


**Fig. A2 Computed species profiles for (a) HXN, (b) HMN and (c) CHX combustions under auto-ignition condition, with initial pressure of 60bar, initial temperature of 950K and $\Phi$ of 1.**

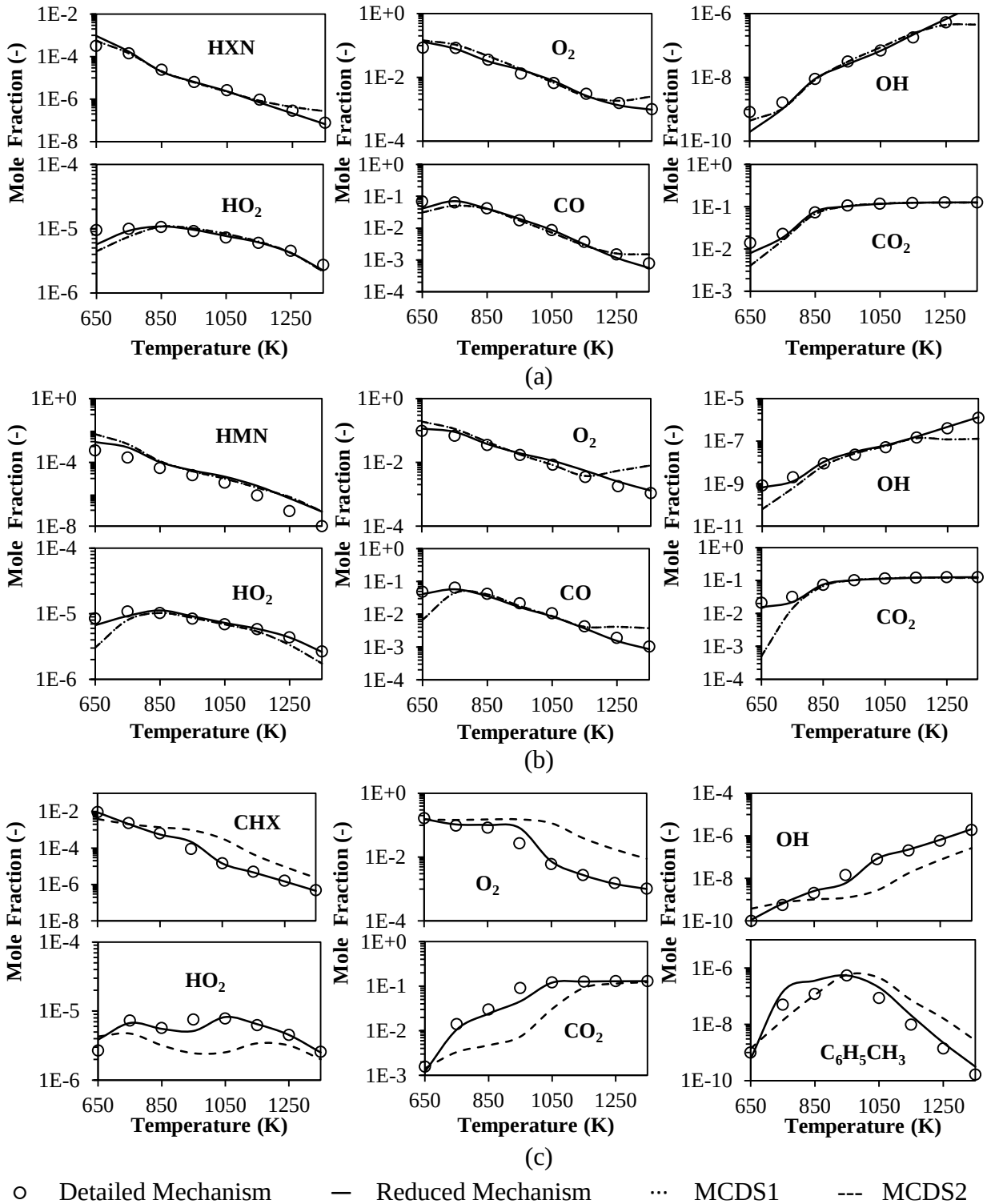


**Fig. A3 Computed species profiles of (a) HXN, (b) HMN and (c) CHX oxidations under JSR condition as a function of temperature, with initial pressure of 60bar and $\Phi$ of 1.**